NIH Public Access
Author Manuscript
Cell Rep. Author manuscript; available in PMC 2014 April 25.

Published in final edited form as:
Cell Rep. 2013 April 25; 3(4): 1199–1212. doi:10.1016/j.celrep.2013.03.031.

Late Recruitment of Synapsin to Nascent Synapses Is Regulated by Cdk5

Courtney Easley-Neal[1], **Javier Fierro Jr.**[1], **JoAnn Buchanan**[2], and **Philip Washbourne**[1,*]
[1]Institute of Neuroscience, University of Oregon, Eugene, OR 97403, USA
[2]Department of Molecular and Cellular Physiology, Stanford University, Stanford, CA 94305, USA

Summary

Synapse formation is a complex process that involves the recruitment and assembly of a myriad of pre- and postsynaptic proteins. Despite being present at every synapse in the vertebrate CNS, little is known about the transport, recruitment, and stabilization of synapsin at nascent synapses during development. We examined the transport and recruitment of synapsin to nascent presynaptic terminals in vivo in the developing zebrafish spinal cord. Synapsin was transported in a transport packet independently of two other presynaptic organelles: synaptic vesicle (SV) protein transport vesicles (STVs) and Piccolo-containing active zone precursor transport vesicles (PTVs). During presynaptic assembly, recruitment of all three transport packets occurred in an ordered sequence: STVs preceded PTVs, which in turn preceded synapsin. Importantly, cyclin-dependent kinase 5 (Cdk5) specifically regulated the late recruitment of synapsin transport packets at synapses. These results point to additional layers of complexity in the established mechanisms of synaptogenesis.

Introduction

Chemical synapses are highly complex sites of neuronal contact at which unidirectional communication occurs. Both pre- and postsynaptic sides of the contact contain up to 1,000 distinct proteins (Valor and Grant, 2007), that must be correctly assembled for the synapse to function. Understanding the mechanisms by which these components are transported and then stabilized at synapses is critical to unraveling developmental disorders such as autism, mental retardation, and schizophrenia (Zoghbi, 2003).

Synapsins are an important component of mature synapses, based on their localization to >99% of synapses in mouse cortex (Micheva et al., 2010). In mammals, these proteins are encoded by three genes, *Synapsin1*, *2*, and *3* (Fornasiero et al., 2010). The synapsins regulate the releasable pool of SVs (Bonanomi et al., 2005) and are phosphorylated by at

©2013 The Authors 1199

*Correspondence: pwash@uoneuro.uoregon.edu.

Supplemental Information: Supplemental Information includes Extended Results, Extended Experimental Procedures, two figures, one table, and two movies and can be found with this article online at http://dx.doi.org/10.1016/j.celrep.2013.03.031.

Licensing Information: This is an open-access article distributed under the terms of the Creative Commons Attribution-NonCommercial-No Derivative Works License, which permits non-commercial use, distribution, and reproduction in any medium, provided the original author and source are credited.

Web Resources: The URLs for data presented herein are as follows:
ClustalW2, http://www.ebi.ac.uk/Tools/msa/clustalw2/
Ensemble Genome, http://www.ensembl.org/index.html
ImageJ, http://rsb.info.nih.gov/ij/
Jalview, http://www.jalview.org/help.html
Stack Reg, http://bigwww.epfl.ch/thevenaz/stackreg/
Synteny Database, http://teleost.cs.uoregon.edu/acos/synteny_db/

NIH-PA Author Manuscript
NIH-PA Author Manuscript
NIH-PA Author Manuscript

NIH-PA Author Manuscript

NIH-PA Author Manuscript

NIH-PA Author Manuscript

least six kinases including cyclin-dependent kinase 5 (Cdk5) and calcium/calmodulin kinase II (CaMKII) (Fornasiero et al., 2010). Phosphorylation can regulate the association of these cytosolic proteins with synaptic vesicles (SVs) and actin (Fornasiero et al., 2010). Although the synapsins were the first SV-associated proteins identified (Fornasiero et al., 2010), the transport of these proteins to synapses has remained understudied. Due to the strong association between SVs and synapsins (Huttner et al., 1983), it has been assumed that they are transported together (Ahmari et al., 2000). Recent imaging studies show that this can be the case (Scott et al., 2011), but quantitative analysis of synapsin transport and an understanding of the mechanisms governing transport and recruitment of synapsins to synapses still remain elusive, especially in vivo.

There are four possible modes of transport by which the synapsins could be conveyed to presynaptic terminals: (1) cytosolic diffusion (Scott et al., 2011), (2) association with SV protein transport vesicles (STVs) (Ahmari et al., 2000; Scott et al., 2011), (3) association with Piccolo-containing active zone precursor transport vesicles (PTVs) (Tao-Cheng, 2007; Zhai et al., 2001), or (4) with an as-yet-unknown transport complex. STVs transport an array of SV proteins including VAMP2/synaptobrevin2 (VAMP2), synaptotagmins, and SV2 (Ahmari et al., 2000; Takamori et al., 2006). STVs vary widely in size from clusters the size of a few SVs to larger tubulovesicular aggregates of SV material (Ahmari et al., 2000; Kraszewski et al., 1995). In contrast, PTVs are more uniform 80 nm dense-core vesicles that carry active zone cytomatrix proteins, as well as proteins involved in calcium sensing and vesicle fusion, such as Piccolo, Bassoon, N-cadherin, and SNAP-25 (Shapira et al., 2003; Zhai et al., 2001). Both STVs and PTVs are transported bidirectionally along axons, pausing for varying lengths of time (Ahmari et al., 2000; Bury and Sabo, 2011; Kraszewski et al., 1995; Sabo et al., 2006; Shapira et al., 2003; Zhai et al., 2001). Cotransport of synapsins with either STVs or PTVs would constitute an efficient delivery mechanism for the synapsins to synapses.

Previous studies examining the trafficking of presynaptic components to CNS synapses have almost exclusively been performed in vitro, due to the lack of an appropriate in vivo model for synapse assembly. Recent live imaging studies in zebrafish (*Danio rerio*) (Jontes et al., 2000, 2004) have suggested that this organism possesses the characteristics necessary to facilitate examination of synaptogenesis in a living vertebrate. Rohon-Beard (RB) sensory neurons in the zebrafish spinal cord lend themselves to live-imaging studies as their central axons are linear, allowing fast imaging within a narrow range of focus (Figures 1A and 1B) (Jontes et al., 2004). These cells transduce the sense of touch (Douglass et al., 2008) to mediate touch-evoked coiling behavior by 1 day postfertilization (dpf) (Saint-Amant and Drapeau, 1998). RB cells form synapses with commissural primary ascending (CoPA) interneurons (Figure 1B) (Downes and Granato, 2006; Gleason et al., 2003) and these AMPA-type glutamate receptor-dependent synapses are sufficient to sustain sensory-motor behavior (Pietri et al., 2009).

In this study, we examined the mechanisms by which synapsin traffics to sites of nascent synapses between RB and CoPA cells in vivo. Live imaging demonstrated that synapsin1 is transported in discrete puncta. Synapsin transport packets moved independently of STV and PTV markers, thus presenting a novel transport packet to consider during presynaptic assembly. Synaptic recruitment of all three transport packets was in a defined sequence: STVs arrived at nascent synapses first, followed by PTVs after an ~30 min delay, and then synapsin after an additional ~30 min had elapsed. We found that Cdk5 was instrumental in regulating recruitment of synapsin to nascent synapses. Thus, our study examines the kinetics and molecular mechanisms of synaptic recruitment of synapsin transport packets in vivo and demonstrates that presynaptic assembly proceeds in a sequential fashion.

NIH-PA Author Manuscript

NIH-PA Author Manuscript

NIH-PA Author Manuscript

Results

Synapsin Localizes at Synapses between RB and CoPA Cells

We began our examination of synapses between sensory RB axons and CoPA cells in the spinal cord of zebrafish embryos at 25 hpf (Figure 1A), a developmental stage at which embryos can respond to touch (Saint-Amant and Drapeau, 1998). By this stage, RB central axons expressing GFP from a *neurogenin1*:GFP transgene (ngn1:GFP; Tg[−3.1ngn1:GFP] sb2) extend along the length of the dorsal longitudinal fascicle (dlf; Figure 1B, arrow in Figure 1C). These axons lie directly adjacent to CoPA interneuron cell bodies, as visualized by immunolabeling with con-1 antibody (Figure 1B, arrowhead in Figure 1C) (Bernhardt et al., 1990).

Immunolabeling with antibodies to synapsins 1 and 2 and postsynaptic density membrane-associated guanylate kinase proteins (MAGUKs) PSD-95, PSD-93, and SAP102 (pan MAGUK antibody) (Meyer et al., 2005) was used to examine the localization of synapsins at synapses between RB axons and CoPA cells at this stage of development. To identify and visualize CoPA cells, we expressed Tau-GFP fusion protein in a mosaic distribution by injecting a neuronal expression vector into fertilized eggs at the one cell stage. The preferential targeting of Tau-GFP to axons facilitated the identification of CoPA cells by virtue of their ascending, commissural axon (Bernhardt et al., 1990). We observed punctate labeling of both synapsin 1/2 and pan MAGUK antibodies at the cell bodies of CoPA cells at 24–26 hpf (Figure 1D, left panel). For considerations of MAGUK labeling specificity, see the Extended Results and Movie S1. When we examined images in which synapsin and MAGUK immunolabeling was overlayed (Figure 1D), we saw colocalization in distinct puncta at CoPA cell bodies, demonstrating that synapsins localize at synapses on CoPAs in the developing zebrafish spinal cord.

As axons from several neuronal populations project in the dlf, including the axons of contralateral CoPA cells, it was conceivable that the synapses located on CoPA cell bodies might represent a mixed population of synapses from RBs, CoPAs, and other neurons. The narrowminded mutation (nrd, *prdm1a*$^{m805/m805}$) disrupts the *prdm1a* gene, resulting in a deficit in neural crest cell development, including loss of the RB cells (Hernandez-Lagunas et al., 2005), while sparing all other neurons examined in the spinal cord (data not shown). *prdm1a*$^{m805/m805}$ embryos showed no punctate immunoreactivity for MAGUKs or synapsin on CoPA cell bodies (Figure 1D, Wild-Type [WT] n = 4, *prdm1a*$^{m805/m805}$ n = 3). We conclude that all synapses containing synapsins that impinge on CoPAs are from RBs at this stage of development.

There are between 50 and 78 RB cells along each side of the entire spinal cord (Eisen and Pike, 1991), but on average only 23 CoPA interneurons (Eisen and Pike, 1991). For our further studies of synapse assembly, it was important to take into account the overall connectivity between RBs and CoPAs. For example, if a given RB synapses with only a subset of CoPA cells, it would be challenging to distinguish the region of axon that synapses with a CoPA cell of interest. To address this, we examined embryos that had been injected with a RB-specific GFP expression vector and in which only a single RB was fluorescently labeled. Immunolabeling with synapsin 1/2 and pan MAGUK antibodies revealed that, at 25 hpf, 87.1% of CoPAs (n = 31 CoPAs from 13 embryos; arrowheads in Figure 1E) had formed synapses with single-labeled RB axons as indicated by synapsin immunoreactivity in the RB axon adjacent to the MAGUK puncta. Furthermore, on average, a single synapse (1.3 ± 0.1; n = 18 CoPAs from 8 embryos) was observed between a RB axon and each CoPA cell. By 28 hpf, we observed as many as 39 postsynaptic puncta at a single CoPA (average = 18.7 ± 2.3; see Figure 3), suggesting that eventually every RB may synapse onto every CoPA within a hemispinal cord. Importantly for our studies, these results suggest that

NIH-PA Author Manuscript

NIH-PA Author Manuscript

NIH-PA Author Manuscript

every RB contacts the overwhelming majority of CoPAs in one side of the spinal cord and that a single synapse forms at each contact site.

Ultrastructure of Immature Synapses on CoPA Cell Bodies

We next examined the ultrastructure of RB-CoPA synapses to determine whether the classical hallmarks of synapses could be resolved at this early developmental time point. We performed transmission electron microscopy on transverse sections of embryos at 25 and 28 hpf. We found that CoPA cells could be identified in cross section due to (1) their cell body shape, (2) their dorsolateral location within the spinal cord, and (3) their proximity to the dlf (Figure 2A). At 25 and 28 hpf, we were able to identify axons forming the dlf lying lateral to CoPA cell bodies. Many of these axons contacted the lateral face of a CoPA cell body (Figures 2B and 2C). At 25 hpf, some axons were contacted by small filopodial extensions from the CoPA cell body, and these contact sites showed accumulations of SVs (Figure 2D, in 3/3 CoPA-like cells examined). Filopodial extensions from the cell bodies of CoPA cells were not observed at 28 hpf (Figures 2B and 2C, 4/4 CoPA-like cells).

At 28 hpf, a few axon profiles directly in contact with the cell body (in 4/4 cells examined) demonstrated accumulations of SVs (Profiles 1 and 2 in Figure 2B). Analysis of contacts with accumulations of SVs at higher magnification revealed an even apposition and a thickening of the pre- and postsynaptic membranes (Figures 2E and 2F). Furthermore, we noted weakly labeled postsynaptic densities, suggesting that these contacts are immature synapses (Ahmari and Smith, 2002). Upon overlay of multiple cell body profiles together with their impinging presynaptic axon terminals, wenoticed that synapses were clustered within the region of the lateral face of the CoPA cells contacted by the dlf (Figure 2C). From these experiments, we conclude that at 25–28 hpf synapse formation is ongoing between axons of the dlf, which we previously identified as being from RBs, and CoPA cells in the zebrafish spinal cord.

Delayed Recruitment of Synapsins

We next examined the time course over which synapsins and SVs accumulated at RB-CoPA synapses. Embryos from transgenic ngn1:GFP zebrafish, which express GFP in RBs, were immunolabeled with antibodies to synapsins and synaptotagmin2b (synaptotagmin), to label SVs and STVs, and to postsynaptic MAGUKs. Embryos were fixed and labeled at 19, 22, 25, and 28 hpf. These ages flank the onset of the touch response at 21 hpf (Pietri et al., 2009; Saint-Amant and Drapeau, 1998), when we would hypothesize that RB-CoPA synapses form and become functional.

At 19 hpf, punctate immunoreactivity for synaptotagmin was seen along the dlf. Colabeling with antibodies that label CoPA cells (con-1) revealed that punctate aggregates of synaptotagmin were adjacent to CoPA cell bodies where they contacted the dlf (Figure 3A). We found an average of 2 (±0.27, n = 8 CoPAs) puncta per CoPA with synaptotagmin immunoreactivity, and this number increased at each developmental time point examined (Figures 3B and 3D). These results suggest that STVs are present in axons at these stages of development and that the number of STVs adjacent to CoPA cell bodies increases over time.

In contrast to the early appearance of STV immunoreactivity, immunolabeling for synapsin was first seen at 22 hpf (Figures 3C and 3D), 3 hr later than SV protein synaptotagmin. A portion of the synapsin labeling was diffuse throughout the dlf, but large, intense puncta were occasionally seen in axons, especially at sites adjacent to CoPA cell bodies (Figure 3C). The numbers of synapsin puncta steadily increased with development (Figures 3C and 3D). To determine what fraction of synapsin puncta were indeed synaptic, we examined MAGUK immunoreactivity. This postsynaptic marker was detected earlier than synapsin, at

NIH-PA Author Manuscript

NIH-PA Author Manuscript

NIH-PA Author Manuscript

19 hpf, and an increasing number of MAGUK puncta were seen in CoPA interneurons at each later time point (Figures 3C and 3D). Importantly, adjacent synapsin and MAGUK puncta were seen at CoPA cell bodies at ~22 hpf (arrowhead, Figures 3C–3F), a time at which these synapses are presumed functional (Pietri et al., 2009). Only a small proportion (4.79% ± 2.21%, n = 16 CoPAs) of the many MAGUK puncta were adjacent to synapsin at 22 hpf, but this proportion steadily grew to over 25% over the next 6 hr of development (Figure 3E). In contrast, the proportion of synapsin puncta that were adjacent to MAGUK proteins was much higher and remained relatively constant overtime, averaging 69–91% (19 hpf, n = 16 CoPAs; 22 hpf, n = 15; 25 hpf, n = 21; 28 hpf, n = 18) over the ages examined (Figure 3F). Based on the different developmental time points at which markers for STVs and synapsin appear, our immunolabeling studies suggest that there is a sequential arrival of synaptic proteins at the RB-CoPA synapse. These results also imply that synapsins and STVs are trafficked independently to synapses.

At this level of analysis, it is important to consider that the 3 hr delay in the arrival of synapsin at RB-CoPA synapses as compared to synaptotagmin may not be solely due to differential trafficking. This delay could also depend on the developmental expression pattern of *synapsin* genes in the zebrafish embryo. We identified and isolated the coding regions of three zebrafish *synapsin* genes, *synapsins1*, *2a*, and *2b*. No ortholog of mammalian synapsin3 was identified in the zebrafish genome, although synapsin2 was present as duplicate co-orthologs (see Table S1 for sequence identity). In situ hybridization at 17, 19, 22, and 25 hpf, revealed that transcripts for these genes did not appear in RBs until 19 hpf (Figure S1). Based on our immunolabeling studies (Figure 3C), we conclude that there appears to be an ~3 hr delay in the generation of synapsin protein. Although the developmental expression pattern explains the late arrival of synapsins at RB-CoPA synapses, it nonetheless underscores the possibility of independent, sequential arrival of STVs and synapsins at the presynaptic terminal.

Synapsin1 Is Transported in Axons Independently of STVs and PTVs

Although previous studies have suggested that synapsin is trafficked to synapses with STVs (Ahmari et al., 2000; Scott et al., 2011) or PTVs (Tao-Cheng, 2007), our immunolabeling data suggest that synapsin may arrive at synapses independently of STVs, and with a delay. To examine how synapsin is transported in RB axons relative to both STVs and PTVs, we imaged fluorescently tagged fusion proteins in RBs in the spinal cords of living zebrafish embryos. We coexpressed synapsin with either fluorescently tagged VAMP2, a membrane protein of SVs, or fluorescently tagged N-cadherin, an integral component of PTVs (Bury and Sabo, 2011; Zhai et al., 2001). We used both GFP and mKate2, a red fluorescent protein, as fluorescent tags to enable imaging of two different constructs simultaneously. For validation of our fluorescently tagged constructs see the Extended Experimental Procedures and Figure S2.

We examined the transport of synapsin-GFP in axons of RB cells between 24 and 26 hpf. We noticed diffuse synapsin-GFP fluorescence throughout the axon and strongly fluorescent puncta of synapsin-GFP, some of which were stabile, but many of which were motile (Movie S2). On average, the diffuse pool of synapsin1-GFP represented only 17.81% ± 3.75% of the total pool of synapsin1-GFP fluorescence. This suggests that the majority of synapsin-GFP is transported as part of a transport packet. We then expressed all chromatically distinct combinations of VAMP2-mKate2, N-cadherin-GFP, synapsin1-GFP, and synapsin1-mKate2 to determine whether synapsin may be transported with STVs or PTVs. When RBs expressing synapsin1-GFP and VAMP2-mKate2 were imaged, we found that the two were transported independently (Figures 4A and 4D), confirming that synapsin1 is not transported by STVs. Puncta expressing only one of the fluorescently tagged markers could be seen moving along the axon (arrowheads Figure 4A). Paused puncta were often

NIH-PA Author Manuscript

NIH-PA Author Manuscript

NIH-PA Author Manuscript

observed where both VAMP2 and synapsin1 were colocalized, however, in many instances (n = 14), one of the two fusion proteins moved away whereas the other remained paused (white and yellow arrows in Figure 4A). This same pattern was seen with the other pairs of presynaptic markers. Ncad-GFP and synapsin1-mKate2 never trafficked together (Figure 4B), and Ncad-GFP and VAMP2-mKate2 rarely did (Figure 4C), suggesting that synapsin, STVs and PTVs are all transported independently. To quantify this effect, we calculated the numbers of puncta that were motile during a 30 min imaging session. For each of the singly labeled presynaptic markers, on average 96.2% of the puncta observed during an imaging session were motile, whereas very few two-color puncta moved (Figure 4D; n = 58 puncta).

We further examined the kinetics of puncta movement. The instantaneous velocities of Ncad-GFP, VAMP2-mKate2, and synapsin1-GFP displayed a wide range as seen in the population histogram (from 0.01–1.44 μm/s, N-cadherin: n = 74 puncta, VAMP2: n = 71 puncta, synapsin n = 55 puncta; Figure 4E). However, the maximal velocities of synapsin1-GFP puncta were significantly below those of Ncad-GFP or VAMP2-mKate2 puncta. synapsin1-GFP puncta did not move faster than 0.57 μm/s, whereas more than 8% of VAMP2 and Ncad puncta moved with higher velocities (VAMP2 = 8.4%, Ncad = 8.1%; Figure 4E), reaching 1.14 and 1.44 μm/s, respectively. This result suggests that synapsin may be transported by motor proteins distinct from those used by STVs and PTVs. Together with the analysis of cotransport, our data demonstrate that PTVs, STVs, and synapsin are transported independently in axons.

Synapsin Is Recruited 1 Hr after STVs

We next investigated the order and timing of synapsin recruitment with respect to STVs and PTVs at individual synapses. We monitored the transport and stabilization of STVs and PTVs overtime and then examined colocalization of endogenous synapsins with paused and motile transport packets. Our results suggest that synapsin is transported independently of STVs and PTVs (Figure 4) and that synapsin might be recruited with a delay when compared to STVs (Figure 3). Thus, we predicted that live imaging of STVs or PTVs and subsequent immunolabeling of synapsins should reveal: (1) that motile transport packets do not colocalize with endogenous synapsins, and (2) that STVs or PTVs, which have stabilized at synapses during imaging, colocalize with synapsins by the end of the imaging period. Furthermore, the averagetime between stabilization of transport packets and the fixation and labeling of synapsin at those puncta would inform us of the time between recruitment of STVs/PTVs and synapsins.

We performed this analysis by recording STV transport and pausing over a 2 hr time period starting at ~24 hpf (Figure 5A). The movies were used to generate a retrospective stability map; a “heat” map that indicates the length of time that each punctum was paused prior to the end of the imaging period and fixation (Figure 5B). This analysis revealed a wide variety of stabilities, ranging from puncta that were not paused at the end of imaging (0 hr, dark blue), puncta that paused during imaging and remained there until the end of imaging (e.g., 0.5 hr, arrow, light blue in stability map), to puncta that were paused for the entire imaging period (>2 hr, arrowhead, magenta).

We used labeling of MAGUKs to determine whether paused fusion-protein positive puncta had stabilized at bona fide synapticsites. When colocalization between MAGUK protein IF and VAMP2-mKate2 puncta was analyzed, we did not find any instances in which VAMP2-mKate2 puncta, that had been paused for <1.5 hr or that were not paused at the end of the imaging period, colocalized with MAGUK puncta (arrow in Figures 5A–5C; n = 7 RB axon segments). Further, we found that only VAMP2-mKate2 puncta that had been paused for at least 1.5 hr prior to fixation were stabilized adjacent to MAGUK puncta (average stability with MAGUK localization = 94.8 min ± 14.7 min, n = 7 RB axon segments and 74 puncta;

NIH-PA Author Manuscript

NIH-PA Author Manuscript

NIH-PA Author Manuscript

Figure 5C). Interestingly, the total fluorescence intensity was highest for VAMP2-mKate2 puncta that had been paused for the longest amount of time (Figure 5D), ~50% of which are synaptic sites, as indicated by the presence of postsynaptic MAGUKs. This 2.7–7.3-fold increase in intensity of long-term paused puncta over newly paused puncta suggests that additional VAMP2-mKate2 positive STVs are added to synaptic sites more than 2 hr after initial pausing. These data suggest that STVs stabilize at nascent synaptic sites and that stabilization precedes accumulation of postsynaptic MAGUK scaffolding proteins by ~1.5 hr.

We next examined whether endogenous synapsin was transported with VAMP2-positive STVs. Although many VAMP2-mKate2 transport packets were moving at the end of the imaging session or had paused up to 30 min before the end of the imaging period (62% of all puncta analyzed), none of these were colocalized with synapsin (arrow Figures 5B and 5E). This confirms that endogenous synapsin does not transport with VAMP2-mKate2 positive STVs.

However, synapsin was colocalized with VAMP2-mKate2 clusters that had been paused for at least 1 hr (arrowhead Figures 5A, 5B and 5E; n = 13 RB axon segments, and 118 puncta). In addition, ~100% of stable VAMP2-mKate2 puncta that had stabilized at MAGUK puncta were also colocalized with synapsin (arrowhead Figures 5A and 5B; n = 7 RB axon segments). As CoPA cells have not yet established dendrites and their cell bodies do not monopolize the dlf, we focused our analysis on potential synaptic sites by examining axonal regions adjacent to CoPA cell bodies (within 2 μm). This analysis revealed that only 30% of motile puncta (t = 0) were in proximity to a CoPA at the time of fixation (Figure 5F). In contrast, the probability that a VAMP2-positive punctum was immobilized at a CoPA was above 50% if it was paused for at least 30 min (Figure 5F). Puncta that had paused for over 2 hr had over 70% probability of being colocalized with a CoPA cell (Figure 5F). We analyzed the percentage of puncta that had paused at CoPAs and that were colocalized with synapsins. One hundred percent of long-term paused puncta at CoPA cells (>2 hr) and ~43% of puncta that had been paused at CoPA cells for ~2 hr were colocalized with synapsin (Figure 5E, gray bars). These data suggest that synapsin is recruited to synaptic sites that have already assembled STVs. Furthermore, we conclude that synapsin and postsynaptic MAGUK proteins are recruited to new synapses with a similar time course.

PTVs Are Recruited before Synapsin

We next examined the time course of synapsin recruitment to the RB-CoPA synapse as compared with PTVs. Live imaging of Ncad-GFP and postimaging IF labeling for synapsin and MAGUKs were performed as previously described. Again, we analyzed puncta that were in close proximity to CoPA cells. Puncta that had been actively trafficking at the end of the imaging period almost never colocalized with synapsin and MAGUKs (Figures 6A–6C), suggesting that endogenous synapsin is not transported with PTVs. We found that Ncad-GFP puncta colocalized with synapsin, on average, 37.6 ± 8.0 min after stabilizing at CoPAs (see arrows Figure 6D; n = 13 RB axon segments and 92 puncta). In comparison, the average time of colocalization after stabilization for VAMP2 was 73.8 ± 12.5 min (Figure 6D; $p < 0.05$, n = 13 RB axon segments and 118 puncta). One hundred percent of Ncad-GFP puncta that colocalized with synapsin were also found to be adjacent to MAGUK puncta. These data suggest that PTVs arrive at synapses ~30 min prior to synapsin, and with a distinct time course to VAMP2 transport packets.

Neuronal Activity Does Not Regulate Synapsin Recruitment

Synapsin localization at mature synapses is tightly regulated by neuronal activity (Lazarevic et al., 2011). To examine the effect of activity on synapsin recruitment to nascent synapses,

NIH-PA Author Manuscript

NIH-PA Author Manuscript

NIH-PA Author Manuscript

we immunolabeled synapsin1/2 and MAGUKs in zebrafish carrying the *macho* mutation (*mao*$^{tt261/tt261}$). This mutation results in a lack of action potentials in RB cells and other sensory neurons due to a reduction in voltage-gated sodium currents (Pineda et al., 2005). Homozygous mutants, as identified by a lack of touch response (Ribera and Nüsslein-Volhard, 1998), demonstrated similar numbers of synapsin puncta at CoPA cells (3.9 ± 0.8 versus 3.2 ± 0.8, $p > 0.5$, n = 5 embryos each) and equivalent colocalization of MAGUK puncta with synapsin (21.3% ± 4.4% versus 25.1% ± 5.6%, $p > 0.5$, n = 5 embryos), as compared to sibling embryos with touch sensitivity (data not shown). This analysis suggests that the transport and stabilization of synapsins at synapses is not dependent on the activity level of RB cells.

Cdk5 Regulates Synapsin Recruitment

A key function of synapsin is to maintain the SV reserve pool, a role that is shared with Cdk5 (Kim and Ryan, 2010). Cdk5 is expressed in zebrafish embryos from the beginning of development, and Cdk5 expression has been shown in the spinal cord at 24 hpf (Kanungo et al., 2007). Furthermore, Cdk5 is highly expressed in RB cells (Kanungo et al., 2009), so we hypothesized that synapsin1 recruitment might be regulated by Cdk5. We tested this hypothesis by inhibiting Cdk5 activity with roscovitine and examined synapsin1 transport or stabilization at synapses. Because synapsins are tightly associated with the actin cytoskeleton at synapses (Fornasiero et al., 2010), we considered other kinases that regulate actin. Thus, we tested an inhibitor of focal adhesion kinase (FAK14), a kinase that stabilizes the presynaptic cytoskeleton (Fabry et al., 2011). We also tested an inhibitor of p38 MAPK (SB203580), a kinase involved in synapse development through cadherins (Ando et al., 2011), which also stabilize the presynaptic actin cytoskeleton (Bozdagi et al., 2004).

We imaged embryos expressing synapsin1-GFP in RB axons that were treated with the inhibitors for 1–3 hr and found that roscovitine treatment caused a significant decrease in the number of paused puncta and a concomitant increase in the number of motile puncta (Figures 7A and 7B; control n = 5 axons and 42 puncta, roscovitine n = 5 axons and 48 puncta). None of the other kinase inhibitors affected transport or pausing of synapsin1-GFP (Figure 7B; SB203580 n = 6 axons and 59 puncta, FAK14 n = 5 axons and 38 puncta). There was no significant difference in the total number of puncta in any condition. Roscovitine treatment did not perturb puncta motility or pausing of VAMP2-mKate2 and N-cadherin-GFP (Figures 7C and 7D), suggesting that Cdk5-regulated stabilization is specific to synapsin transport packets.

To characterize the effect of roscovitine on endogenous synapsin and STVs, we examined immunoreactivity for synapsin1/2, synaptotagmin2b, and MAGUKs in WT embryos treated with roscovitine from 23–26 hpf. The colocalization ofMAGUK puncta with synapsin puncta was significantly decreased in the roscovitin-treated embryos (Figures 7E and 7F; control n = 9 embryos, roscovitine n = 10 embryos). The average number of puncta per CoPA in the roscovitine treatment condition was not significantly affected for any of the markers (Figure 7G; control: synapsin1/2 n = 29, synaptotagmin2b n = 6, MAGUKs n = 29, roscovitine: synapsin 1/2 n = 42, synaptotagmin2b n = 10, MAGUKs n = 42), although there was a small, but insignificant, decrease in the total number of synapsin puncta in the roscovitine treatment condition ($p = 0.096$; Figure 7G). These results implicate Cdk5 kinase activity in the stabilization of synapsin transport packets at nascent synapses.

Roscovitine can also inhibit Cdk1 and 2 (Knockaert et al., 2002), so to further characterize the role of Cdk5 in the recruitment of synapsin to synapses we used morpholine-modified antisense oligonucleotides (MOs) to specifically knockdown Cdk5 levels (Tanaka et al., 2012). We monitored the transport of synapsin1 transport packets in RB axons in the presence of MO. Cdk5 knockdown caused a reduction in the ratio of immotile to total

NIH-PA Author Manuscript

NIH-PA Author Manuscript

NIH-PA Author Manuscript

puncta (Figure 7H; control = 0.5 ± 0.07, MO = 0.3 ± 0.01, $p < 0.05$, n = 7 axons for all conditions), similarly to roscovitine treatment (Figure 7B). This effect was rescued by coinjecting mRNA encoding human Cdk5 (MO + RNA = 0.5 ± 0.04, $p < 0.05$). Furthermore, knockdown reduced the colocalization of endogenous synapsins and postsynaptic MAGUKs, as revealed by immunolabeling of Cdk5 MO-injected embryos (Figure 7I; $p < 0.05$; control n = 12, MO n = 11, MO + RNA n = 14 CoPAs). Cdk5 knockdown also resulted in a significant reduction in the number of synapsin puncta on CoPA cells (Figure 7J; $p < 0.001$), but did not result in a significant reduction in the other presynaptic marker, synaptotagmin (Figure 7J; $p > 0.05$). Taken together, these data suggest that Cdk5 specifically regulates the stabilization of synapsin transport packets at synapses.

Cdk5 could play a permissive role in allowing synapsin transport packets to stop at synapses. Alternatively, Cdk5 might take on an instructional role in the recruitment of synapsin to nascent presynaptic terminals. In this case, local activation of Cdk5 would be necessary for stabilization of synapsins. To distinguish between the two possibilities, we ectopically and constitutively activated Cdk5 by expressing RNA encoding human Cdk5 and human p25C in developing zebrafish embryos and analyzed localization of synapsins at synapses. p25C is a cleavage fragment of p35, an activator of Cdk5. Association of p25C with Cdk5 results in prolonged, ectopic activation of Cdk5 (Cheung and Ip, 2007). Expression of Cdk5 or p25C alone had no significant effect on the localization of synapsins at synaptic sites (Figure 7I, $p > 0.05$). In contrast, coexpression of Cdk5 and p25C resulted in a significant reduction in the colocalization of synapsin with postsynaptic MAGUKs (Figure 7I, $p < 0.005$). The localization of MAGUK puncta at CoPA cells was not affected by these manipulations (Figure 7J, $p > 0.05$). Although Cdk5 knockdown did not affect the localization of synaptotagmin puncta at CoPA cells, all manipulations resulting in Cdk5 hyperactivity (i.e., Cdk5 RNA or p25C RNA injection) resulted in an ~25% decrease in synaptotagmin puncta number (Figure 7J). This suggests that Cdk5 activity may be sufficient, but not necessary, to restrict STV recruitment. This mechanism is distinct from the role of Cdk5 on synapsin localization at synapses in that it persists when Cdk5 activity is ectopic. Our data suggest that the activation of Cdk5 is tightly controlled, and that the localization of Cdk5 activity is critical for synapsin localization to synapses.

Discussion

In the current study, we have made three important advances in understanding the recruitment of presynaptic components to nascent synapses. First, we have shown that synapsin1, an important regulator of SV release and the SV reserve pool, is transported as part of a distinct complex to nascent synapses, independently of STVs and PTVs. Second, our studies have revealed a defined sequence in the recruitment of presynaptic transport packets to a nascent synapse. Third, we identify Cdk5 as a specific regulator of synapsin recruitment to nascent presynaptic terminals. Using the RB-CoPA synapse in zebrafish spinal cord as a model glutamatergic synapse (Figures 1 and 2), we first showed a time delay between the recruitment of STV proteins and synapsin to presynaptic terminals by IF labeling (Figure 3). We demonstrated using three independent methods that synapsin is transported in discrete puncta independently of STVs and PTVs: by live 2-color imaging of synapsin1 with STV and PTV markers (Figure 4), by live imaging of STVs or PTVs with postimaging IF labeling of endogenous synapsins (Figures 5 and 6), and through the specificity of Cdk5 regulation of synapsin stabilization (Figure 7).

To date, the presynaptic terminal has not been described to assemble with a defined sequence of recruitment. Our experiments using time-lapse imaging with post hoc immunolabeling (Figures 5 and 6) and immunolabeling at different developmental times (Figure 3) argue for a defined sequence in presynaptic assembly. We present evidence that a

NIH-PA Author Manuscript

NIH-PA Author Manuscript

NIH-PA Author Manuscript

primary step in synaptic assembly is the recruitment of STVs. PTVs are then added with an ~30 min delay. Subsequently, synapsin transport packets, also with an ~30 min delay, are recruited to the nascent terminal. Additionally, our studies suggest that a later step in assembly (>2 hr) may be the aggregation of additional STVs (Figure 5D). Given the role of synapsins in tethering synaptic vesicles at synapses (Fornasiero et al., 2010) and pause sites (Sabo et al., 2006), it is possible that the accumulation of synaptic vesicle components over 2 hr after initial STV recruitment is dependent on the prior accumulation of synapsin transport packets at synapses.

Our results concerning the method of synapsin transport were surprising for two reasons: (1) synapsin is tightly associated with SVs at mature synapses (Huttner et al., 1983), suggesting that synapsin could be transported by STVs during synapse formation (Scott et al., 2011); and (2) if synapsin were not transported with STVs, it would be expected that this cytosolic protein might diffuse and then aggregate at synapses (Scott et al., 2011), much like PSD-95 (Barrow et al., 2009; Bresler et al., 2001). Although it is important to note that our techniques may not detect the entire pool of available synapsin, our studies do suggest that a certain proportion of synapsin1 is associated either with a distinct vesicular transport organelle or with a complex of cytosolic proteins that may be transported by a discrete set of motor proteins (Figure 4E). Scott et al. (2011) suggest that synapsin can traffic along axons either slowly as part of molecular motor-driven cytosolic protein aggregates, or quickly by associating with transport packets carrying the integral SV protein synaptophysin. The slow cytosolic transport of synapsin in cultured hippocampal neurons was diffuse and not clearly punctate, and was much slower than that which we have observed here (Scott et al., 2011). Although it is unclear what proportion of synapsin clusters are cotransported with synaptophysin (Scott et al., 2011), it will be interesting to determine whether this is also a rare event (that we observed <10% of the time; Figure 4D) in hippocampal neurons, or whether this represents a difference in transport mechanisms between cultured hippocampal neurons and sensory neurons in vivo.

Previous studies of the transport of presynaptic components to new synapses have remained contradictory. Two reports suggest that all of the proteins necessary to form a presynaptic terminal, including STV proteins, active zone proteins, and synapsins are cotransported (Ahmari et al., 2000; Tao-Cheng, 2007). On the other hand, immuno-isolated PTVs containing only active zone proteins, but not VAMP2 or other SV proteins such as synaptotagmin and synaptophysin, are transported to synapses (Shapira et al., 2003; Zhai et al., 2001). Recently, Bury and Sabo (2011) showed that a significant fraction of STVs and PTVs cotransport along axons of neurons in culture. Although we see that STV and PTV markers can cotransport in our system, we find that the majority of the time, STVs and PTVs traffic separately in vivo (Figure 4). Similarly to the study by Bury and Sabo (2011), we found that STVs and PTVs copause at the same sites. Our data suggest that at certain times during transport, all three transport packets, STVs, PTVs, and synapsin transport packets, pause at common sites along the axon (Figures 4A–4C). This would explain the colocalization of a wide variety of presynaptic proteins in postimaging IF and immuno-EM studies (Ahmari et al., 2000; Tao-Cheng, 2007). In fact, interaction between all three transport packets, STVs, PTVs, and synapsin transport packets, at such reservoirs may regulate their pausing, as deletion of the synapsins significantly decreases pause duration of STVs (Sabo et al., 2006). One would, thus, predict that a decrease in pausing of synapsin transport packets (Figure 7) might result in a decrease in STV pausing. However, based on our data regarding the localization of Cdk5 activity (Figure 7I), we conclude that pausing of synapsin transport packets is only compromised at synaptic sites when Cdk5 activity is reduced, and not at nonsynaptic pause sites.

NIH-PA Author Manuscript

NIH-PA Author Manuscript

NIH-PA Author Manuscript

Transport properties of STVs and PTVs were indistinguishable in our experiments (Figure 4). This is in line with a similar study also performed in RB cells using N-cadherin and VAMP fusion proteins (Jontes et al., 2004). In that study, the authors examined the deposition of Ncad-GFP and VAMP-GFP puncta in RB axons in the wake of an extending growth cone and found that both were transported with similar kinetics (Jontes et al., 2004). Because the postsynaptic component was not identified in these experiments, it is possible that these depositions were just paused, an occurrence that was frequently observed in our current study (Figures 5 and 6), and not stabilized at a synapse. This presynaptic precursor material may be deposited behind the advancing growth cone at predefined sites along the axon such as those described by Sabo et al. (2006). From these sites, STVs and PTVs could then be recruited to developing synapses, before these sites eventually also become synapses (Sabo et al., 2006).

In addition to regulating axonal transport of various cargoes, including neurofilament monomers (Cheung and Ip, 2007), Cdk5 has been implicated in regulating a number of aspects of synapse formation. Here, we now show that Cdk5 specifically regulates presynaptic recruitment of synapsin transport packets. In nematodes, Cdk5 was shown to regulate presynaptic assembly (Park et al., 2011), but, in contrast to our data, Cdk5 appears to play a more comprehensive role in these invertebrates. Perhaps this difference suggests that regulation of the synapsin transport packet by Cdk5 may be an evolutionarily conserved mechanism; and that subsequent millennia of evolution have brought additional layers of complexity in the assembly and in the regulation of the assembly of synapses in vertebrates. It is also possible that our manipulations did not entirely abrogate Cdk5 activity and that STV or PTV recruitment may require minimal Cdk5 activity. However, our data suggest, that STV recruitment might be negatively regulated by Cdk5, as Cdk5 overexpression or Cdk5 activation resulted in less synaptotagmin puncta at CoPA cells (Figure 7J).

In trying to understand the underlying molecular mechanism of synapsin1 recruitment, it is important to consider that synapsin1 is highly phosphorylated (Fornasiero et al., 2010). Cdk5 can phosphorylate two serine residues in mammalian synapsin1 (S549, S551) (Matsubara et al., 1996) and one of these sites is conserved in zebrafish synapsin1 (S512). Thus, it may be tempting to assume that direct phosphorylation of synapsin by Cdk5 regulates its recruitment to synapses by dissociation from the carrier proteins. However, close examination of live imaging of synapsin transport (Figure 4 and data not shown) suggests that synapsin transport packets stop, rather than disassemble. Therefore, we propose that Cdk5 regulates synapsin recruitment by phosphorylating one of its many other substrates, such as motor proteins or cargo adapters, for example CASK (Samuels et al., 2007).

Importantly, our data shine a spotlight on a potential local mechanism by which presynaptic transport packets may be stabilized at synapses. Activation of a cascade of kinases in the axon, triggered by upstream synaptogenic events, might regulate the sequential recruitment of individual presynaptic components at nascent synaptic sites. It will be critical to unravel these regulatory mechanisms governing synapse assembly to completely understand synapse formation and the pathologies that affect this process.

Experimental Procedures

Analysis of Zebrafish *Synapsin* Genes

To obtain transcripts for the coding sequences for zebrafish *synapsins*, predicted sequences were identified using the Ensemble Genome browser. Three predicted *synapsin* gene transcripts were identified. For further details see Extended Experimental Procedures.

NIH-PA Author Manuscript

NIH-PA Author Manuscript

NIH-PA Author Manuscript

Zebrafish Husbandry

All zebrafish embryos, larvae, and adults were raised and maintained at 28.5°C according to standard protocols (Westerfield, 2000). Lines used include AB/Tübingen, *neurogenin1:GFP* [*Tg(−3.1ngn1:GFP)sb2]*, *narrowminded* (*nrd*^{m805}), *macho* (*mao*^{tt261}), *s1102t:GAL4/UAS:Kaede* [*Et(−1.5hsp70l:Gal4-VP16)s1102t;Tg(UAS-E1b:Kaede)s1999t*]. For details on genotyping and injection, see the Extended Experimental Procedures.

Imaging

Live imaging was performed at room temperature on a spinning disk microscope (McBain Instruments, Simi Valley, Ca) using a Leica 63× oil objective (1.40 NA). All live imaging data were acquired using Volocity software and a Hamamatsu EMCCD camera. All IF was imaged on an inverted Nikon TU-2000 microscope with an EZ-C1 confocal system (Nikon) with either a 40× objective (0.95 NA) or a 100× oil-immersion objective (1.45 NA). For further details on imaging techniques, see the Extended Experimental Procedures.

Immunofluorescence Labeling

Immunofluorescence (IF) labeling was performed by fixing embryos in 4% paraformaldehyde for 1.5 hr. After rinsing in PBS with 0.1% Triton X-100 (PBST), embryos were blocked in block buffer: PBS with 1% BSA, 1% DMSO, 2% goat serum, and 0.1% Triton X-100. Embryos were incubated in primary antibodies in block buffer overnight at 4°C, washed three times in PBST, and incubated with secondary antibodies for 5 hr at room temperature. For antibodies, see the Extended Experimental Procedures.

Analysis

Analysis of imaging data was performed on maximum intensity projections for all fixed images and live movies. Synaptic puncta were selected and counted using Image Pro Plus software as described previously (Washbourne et al., 2002). Stability maps were generated by identifying paused puncta in kymographs made in Image J (Figures 5 and 6) (Rasband, 1997–2011). All graphs were prepared in Microsoft Excel, and statistics were analyzed using an unpaired 2-tailed Student's t test. For further details on image analysis, refer to the Extended Experimental Procedures.

Electron Microscopy

Zebrafish embryos at 25 and 28 hpf were anesthetized with 0.003% tricaine and then fixed and processed for electron microscopy (EM) essentially as described previously (Jontes et al., 2000). Silver thin sections (70 nm) were placed on 200 mesh hexagonal copper grids and examined unstained in a JEOL 100 CX electron microscope at 80 kV. Images were taken using a CCD digital camera system (XR-100 from AMT, Danvers, MA). For the full EM protocol, see the Extended Experimental Procedures.

Supplementary Material

Refer to Web version on PubMed Central for supplementary material.

Acknowledgments

We thank Dmitry Chudakov and Evrogen for making mKate2 available to us prior to initial publication. We thank Thomas Pietri for cloning the zebrafish VAMP2 sequence and generating UAS:GFP and UAS:mKate2. We thank Judith Eisen, Tory Herman, Alexandra Tallafuss, and A. Kimberley McAllister for comments on the manuscript. We thank James Jontes for UAS:N-cadherin-GFP, Judith Eisen for the pBS SK FL-islet1, Steve Goldman for the NBT:Tau-GFP, Kristin Artinger for the *nrd*^{m805} zebrafish line, Herwig Baier for the *s1102t:GAL4/UAS:Kaede* line, and John Kuwada for con-1 antibody. We thank Chris Doe for generously allowing us the use of the spinning

NIH-PA Author Manuscript

NIH-PA Author Manuscript

NIH-PA Author Manuscript

disk microscope. This work was supported by R01NS065795 from the National Institute of Neurological Disorders and Stroke (P.W.) and by a Developmental Biology Training Grant, NIH 5-T32-HD07348 (C.E.-N.).

References

Ahmari SE, Smith SJ. Knowing a nascent synapse when you see it. Neuron. 2002; 34:333–336. [PubMed: 11988164]

Ahmari SE, Buchanan J, Smith SJ. Assembly of presynaptic active zones from cytoplasmic transport packets. Nat Neurosci. 2000; 3:445–451. [PubMed: 10769383]

Ando K, Uemura K, Kuzuya A, Maesako M, Asada-Utsugi M, Kubota M, Aoyagi N, Yoshioka K, Okawa K, Inoue H, et al. N-cadherin regulates p38 MAPK signaling via association with JNK-associated leucine zipper protein: implications for neurodegeneration in Alzheimer disease. J Biol Chem. 2011; 286:7619–7628. [PubMed: 21177868]

Barrow SL, Constable JR, Clark E, El-Sabeawy F, McAllister AK, Washbourne P. Neuroligin1: a cell adhesion molecule that recruits PSD-95 and NMDA receptors by distinct mechanisms during synaptogenesis. Neural Dev. 2009; 4:17. [PubMed: 19450252]

Bernhardt RR, Chitnis AB, Lindamer L, Kuwada JY. Identification of spinal neurons in the embryonic and larval zebrafish. J Comp Neurol. 1990; 302:603–616. [PubMed: 1702120]

Bonanomi D, Menegon A, Miccio A, Ferrari G, Corradi A, Kao HT, Benfenati F, Valtorta F. Phosphorylation of synapsin I by cAMP-dependent protein kinase controls synaptic vesicle dynamics in developing neurons. J Neurosci. 2005; 25:7299–7308. [PubMed: 16093379]

Bozdagi O, Valcin M, Poskanzer K, Tanaka H, Benson DL. Temporally distinct demands for classic cadherins in synapse formation and maturation. Mol Cell Neurosci. 2004; 27:509–521. [PubMed: 15555928]

Bresler T, Ramati Y, Zamorano PL, Zhai R, Garner CC, Ziv NE. The dynamics of SAP90/PSD-95 recruitment to new synaptic junctions. Mol Cell Neurosci. 2001; 18:149–167. [PubMed: 11520177]

Bury LA, Sabo SL. Coordinated trafficking of synaptic vesicle and active zone proteins prior to synapse formation. Neural Dev. 2011; 6:24. [PubMed: 21569270]

Cheung ZH, Ip NY. The roles of cyclin-dependent kinase 5 in dendrite and synapse development. Biotechnol J. 2007; 2:949–957. [PubMed: 17526057]

Douglass AD, Kraves S, Deisseroth K, Schier AF, Engert F. Escape behavior elicited by single, channelrhodopsin-2-evoked spikes in zebrafish somatosensory neurons. Curr Biol. 2008; 18:1133–1137. [PubMed: 18682213]

Downes GB, Granato M. Supraspinal input is dispensable to generate glycine-mediated locomotive behaviors in the zebrafish embryo. J Neurobiol. 2006; 66:437–451. [PubMed: 16470684]

Eisen JS, Pike SH. The spt-1 mutation alters segmental arrangement and axonal development of identified neurons in the spinal cord of the embryonic zebrafish. Neuron. 1991; 6:767–776. [PubMed: 2025428]

Fabry B, Klemm AH, Kienle S, Schäffer TE, Goldmann WH. Focal adhesion kinase stabilizes the cytoskeleton. Biophys J. 2011; 101:2131–2138. [PubMed: 22067150]

Fornasiero EF, Bonanomi D, Benfenati F, Valtorta F. The role of synapsins in neuronal development. Cell Mol Life Sci. 2010; 67:1383–1396. [PubMed: 20035364]

Gleason MR, Higashijima S, Dallman J, Liu K, Mandel G, Fetcho JR. Translocation of CaM kinase II to synaptic sites in vivo. Nat Neurosci. 2003; 6:217–218. [PubMed: 12563265]

Hernandez-Lagunas L, Choi IF, Kaji T, Simpson P, Hershey C, Zhou Y, Zon L, Mercola M, Artinger KB. Zebrafish narrowminded disrupts the transcription factor prdm1 and is required for neural crest and sensory neuron specification. Dev Biol. 2005; 278:347–357. [PubMed: 15680355]

Huttner WB, Schiebler W, Greengard P, De Camilli P. Synapsin I (protein I), a nerve terminal-specific phosphoprotein III. Its association with synaptic vesicles studied in a highly purified synaptic vesicle preparation. J Cell Biol. 1983; 96:1374–1388. [PubMed: 6404912]

Jontes JD, Buchanan J, Smith SJ. Growth cone and dendrite dynamics in zebrafish embryos: early events in synaptogenesis imaged in vivo. Nat Neurosci. 2000; 3:231–237. [PubMed: 10700254]

Jontes JD, Emond MR, Smith SJ. In vivo trafficking and targeting of N-cadherin to nascent presynaptic terminals. J Neurosci. 2004; 24:9027–9034. [PubMed: 15483121]

NIH-PA Author Manuscript

NIH-PA Author Manuscript

NIH-PA Author Manuscript

Kanungo J, Li BS, Goswami M, Zheng YL, Ramchandran R, Pant HC. Cloning and characterization of zebrafish (Danio rerio) cyclindependent kinase 5. Neurosci Lett. 2007; 412:233–238. [PubMed: 17178437]

Kanungo J, Zheng YL, Mishra B, Pant HC. Zebrafish Rohon-Beard neuron development: cdk5 in the midst. Neurochem Res. 2009; 34:1129–1137. [PubMed: 19067160]

Kim SH, Ryan TA. CDK5 serves as a major control point in neurotransmitter release. Neuron. 2010; 67:797–809. [PubMed: 20826311]

Knockaert M, Greengard P, Meijer L. Pharmacological inhibitors of cyclin-dependent kinases. Trends Pharmacol Sci. 2002; 23:417–425. [PubMed: 12237154]

Kraszewski K, Mundigl O, Daniell L, Verderio C, Matteoli M, De Camilli P. Synaptic vesicle dynamics in living cultured hippocampal neurons visualized with CY3-conjugated antibodies directed against the lumenal domain of synaptotagmin. J Neurosci. 1995; 15:4328–4342. [PubMed: 7540672]

Lazarevic V, Schöne C, Heine M, Gundelfinger ED, Fejtova A. Extensive remodeling of the presynaptic cytomatrix upon homeostatic adaptation to network activity silencing. J Neurosci. 2011; 31:10189–10200. [PubMed: 21752995]

Matsubara M, Kusubata M, Ishiguro K, Uchida T, Titani K, Taniguchi H. Site-specific phosphorylation of synapsin I by mitogen-activated protein kinase and Cdk5 and its effects on physiological functions. J Biol Chem. 1996; 271:21108–21113. [PubMed: 8702879]

Meyer MP, Trimmer JS, Gilthorpe JD, Smith SJ. Characterization of zebrafish PSD-95 gene family members. J Neurobiol. 2005; 63:91–105. [PubMed: 15660367]

Micheva KD, Busse B, Weiler NC, O'Rourke N, Smith SJ. Single-synapse analysis of a diverse synapse population: proteomic imaging methods and markers. Neuron. 2010; 68:639–653. [PubMed: 21092855]

Park M, Watanabe S, Poon VY, Ou CY, Jorgensen EM, Shen K. CYY-1/cyclin Y and CDK-5 differentially regulate synapse elimination and formation for rewiring neural circuits. Neuron. 2011; 70:742–757. [PubMed: 21609829]

Pietri T, Manalo E, Ryan J, Saint-Amant L, Washbourne P. Glutamate drives the touch response through a rostral loop in the spinal cord of zebrafish embryos. Dev Neurobiol. 2009; 69:780–795. [PubMed: 19634126]

Pineda RH, Heiser RA, Ribera AB. Developmental, molecular, and genetic dissection of INa in vivo in embryonic zebrafish sensory neurons. J Neurophysiol. 2005; 93:3582–3593. [PubMed: 15673553]

Rasband, WS. ImageJ. Bethesda, MD: U.S. National Institutes of Health; 1997–2011.

Ribera AB, Nüsslein-Volhard C. Zebrafish touch-insensitive mutants reveal an essential role for the developmental regulation of sodium current. J Neurosci. 1998; 18:9181–9191. [PubMed: 9801358]

Sabo SL, Gomes RA, McAllister AK. Formation of presynaptic terminals at predefined sites along axons. J Neurosci. 2006; 26:10813–10825. [PubMed: 17050720]

Saint-Amant L, Drapeau P. Time course of the development of motor behaviors in the zebrafish embryo. J Neurobiol. 1998; 37:622–632. [PubMed: 9858263]

Samuels BA, Hsueh YP, Shu T, Liang H, Tseng HC, Hong CJ, Su SC, Volker J, Neve RL, Yue DT, Tsai LH. Cdk5 promotes synaptogenesis by regulating the subcellular distribution of the MAGUK family member CASK. Neuron. 2007; 56:823–837. [PubMed: 18054859]

Scott DA, Das U, Tang Y, Roy S. Mechanistic logic underlying the axonal transport of cytosolic proteins. Neuron. 2011; 70:441–454. [PubMed: 21555071]

Shapira M, Zhai RG, Dresbach T, Bresler T, Torres VI, Gundelfinger ED, Ziv NE, Garner CC. Unitary assembly of presynaptic active zones from Piccolo-Bassoon transport vesicles. Neuron. 2003; 38:237–252. [PubMed: 12718858]

Takamori S, Holt M, Stenius K, Lemke EA, Grønborg M, Riedel D, Urlaub H, Schenck S, Brügger B, Ringler P, et al. Molecular anatomy of a trafficking organelle. Cell. 2006; 127:831–846. [PubMed: 17110340]

Tanaka H, Morimura R, Ohshima T. Dpysl2 (CRMP2) and Dpysl3 (CRMP4) phosphorylation by Cdk5 and DYRK2 is required for proper positioning of Rohon-Beard neurons and neural crest cells during neurulation in zebrafish. Dev Biol. 2012; 370:223–236. [PubMed: 22898304]

NIH-PA Author Manuscript

NIH-PA Author Manuscript

NIH-PA Author Manuscript

Tao-Cheng JH. Ultrastructural localization of active zone and synaptic vesicle proteins in a preassembled multi-vesicle transport aggregate. Neuroscience. 2007; 150:575–584. [PubMed: 17977664]

Valor LM, Grant SG. Integrating synapse proteomics with transcriptional regulation. Behav Genet. 2007; 37:18–30. [PubMed: 16977502]

Washbourne P, Bennett JE, McAllister AK. Rapid recruitment of NMDA receptor transport packets to nascent synapses. Nat Neurosci. 2002; 5:751–759. [PubMed: 12089529]

Westerfield, M. The Zebrafish Book. Fourth. Eugene, OR: Institute for Neuroscience, University of Oregon; 2000.

Zhai RG, Vardinon-Friedman H, Cases-Langhoff C, Becker B, Gundelfinger ED, Ziv NE, Garner CC. Assembling the presynapticactive zone: a characterization of an active one precursor vesicle. Neuron. 2001; 29:131–143. [PubMed: 11182086]

Zoghbi HY. Postnatal neurodevelopmental disorders: meeting at the synapse? Science. 2003; 302:826–830. [PubMed: 14593168]

NIH-PA Author Manuscript
NIH-PA Author Manuscript
NIH-PA Author Manuscript

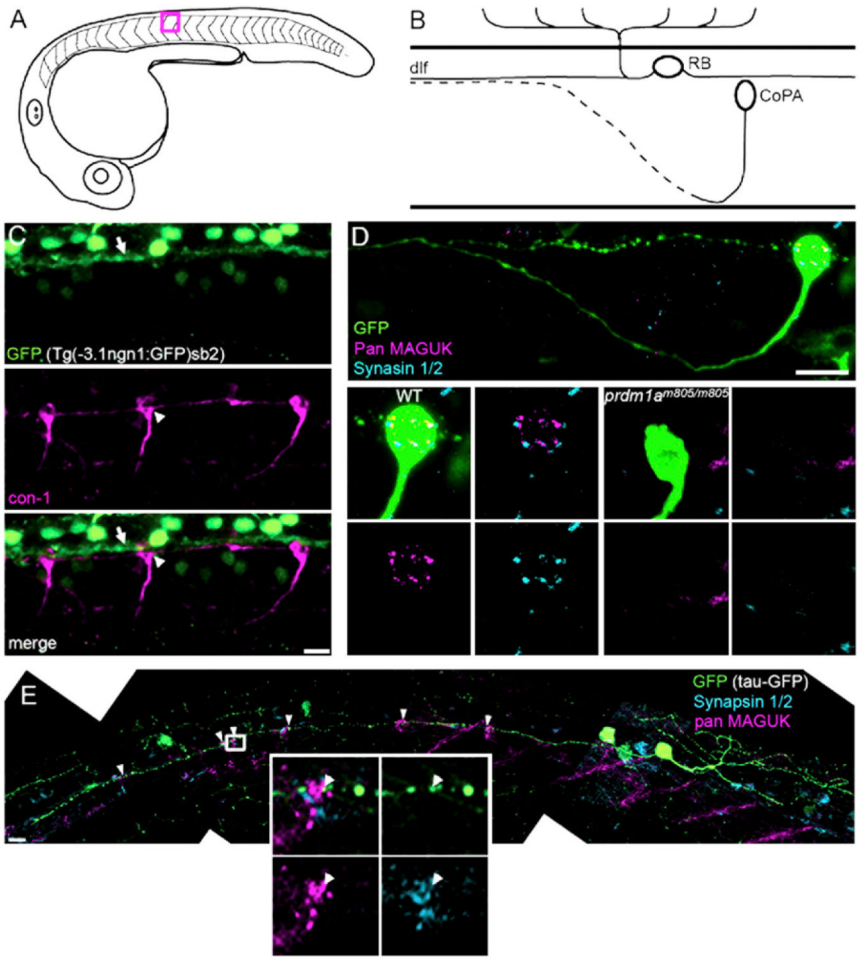

Figure 1. RBs Synapse onto CoPA Interneurons

(A) Diagram of a lateral view of a 25 hpf zebrafish embryo. Studies were performed between segments 11 and 15. Red box outlines segment 12, the region represented in (B).

(B) Diagram depicting the cell body location and axon trajectories of an RB cell and a CoPA cell, in a lateral view of the developing spinal cord. The dotted axon represents a contralateral projection.

(C) CoPA cell bodies (white arrowhead), labeled with con-1 antibody (magenta), were in close proximity to RB axons expressing GFP (white arrow), in ngn1:GFP transgenic embryos. Scale bar represents 10 μm.

(D) pan MAGUK (magenta) and synapsin 1/2 (cyan) immunolabeling on WT and prdm$^{m805/m805}$ embryos with Tau-GFP-labeled CoPA cells. Top panel: shows axon projections and cell body of a CoPA cell in WT embryo. The cell body is shown at higher magnification in bottom left 4 panels, to highlight overlap of pre and postsynaptic puncta. Lower right four panels: no pre- or postsynaptic puncta were seen on CoPA cell bodies in prdm$^{m805/m805}$ embryos, lacking RB cells. Scale bar represents 10 μm.

(E) Composite image of a RB cell expressing GFP (green), including the entire central axon extending rostrally, with labeling for synapsin 1/2 (cyan) and pan MAGUK (magenta). Distinct clusters of colocalized pan MAGUK and synapsin 1/2 immunofluorescence were at CoPA cell bodies, see arrowheads. Inset shows distinct MAGUK and synapsin 1/2 puncta, arrowhead indicates a MAGUK puncta adjacent to a synapsin 1/2 puncta that is within a varicosity in the GFP-expressing RB axon. Scale bar represents 10 μm. See also Movie S1.

NIH-PA Author Manuscript

NIH-PA Author Manuscript

NIH-PA Author Manuscript

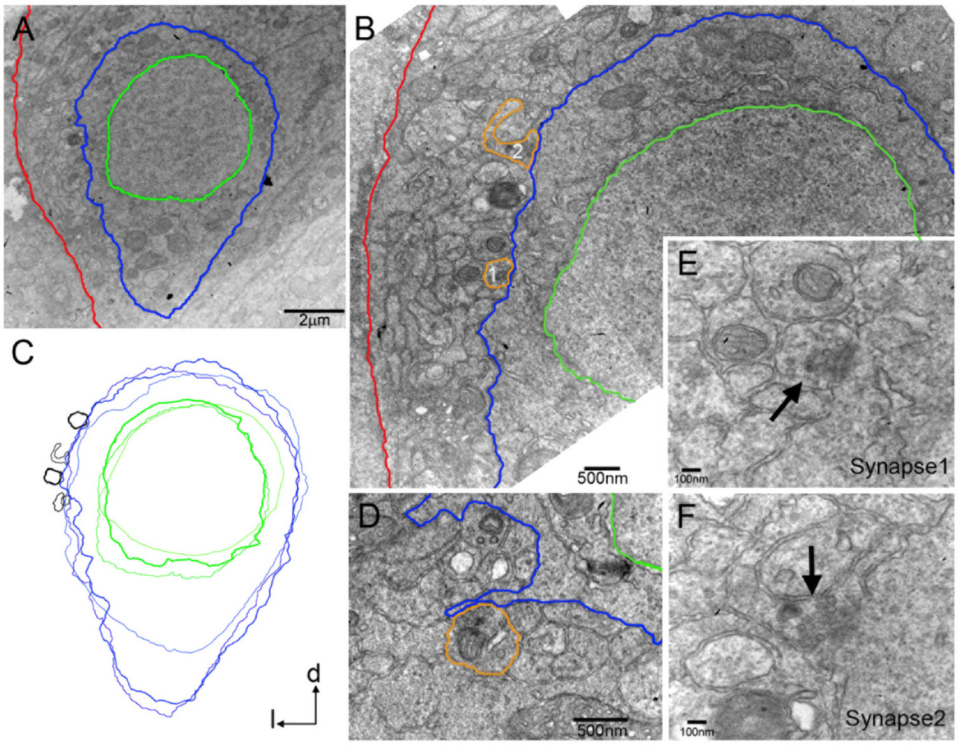

Figure 2. Axosomatic Synapses on CoPA-Like Cells

(A) Electron micrograph of a transverse section of the zebrafish embryo at 28 hpf. CoPA-like cells were identified based on their cell body shape and dorso-lateral location in the spinal cord. The plasma membrane and nuclear envelope were traced inblue and green for clarity, respectively. The basal lamina of the spinal cord is in red.

(B) Synapses (orange tracing) from axons in the dlf were identified on the CoPA-like cell body in (A) (see E and F for higher magnification).

(C) Synapses were found on the lateral face of CoPA-like cells in a stereotypical location, as demonstrated by an overlay of three cell profiles with their synapses (black).

(D) At 25 hpf, synapses were located on small filopodial extensions from the cell body.

(E and F) Higher magnification images of synapse1 (E) and synapse2 (F) in (B), with accumulations of synaptic vesicles (arrows), smooth apposed synaptic membranes and weakly labeled postsynaptic densities.

NIH-PA Author Manuscript

NIH-PA Author Manuscript

NIH-PA Author Manuscript

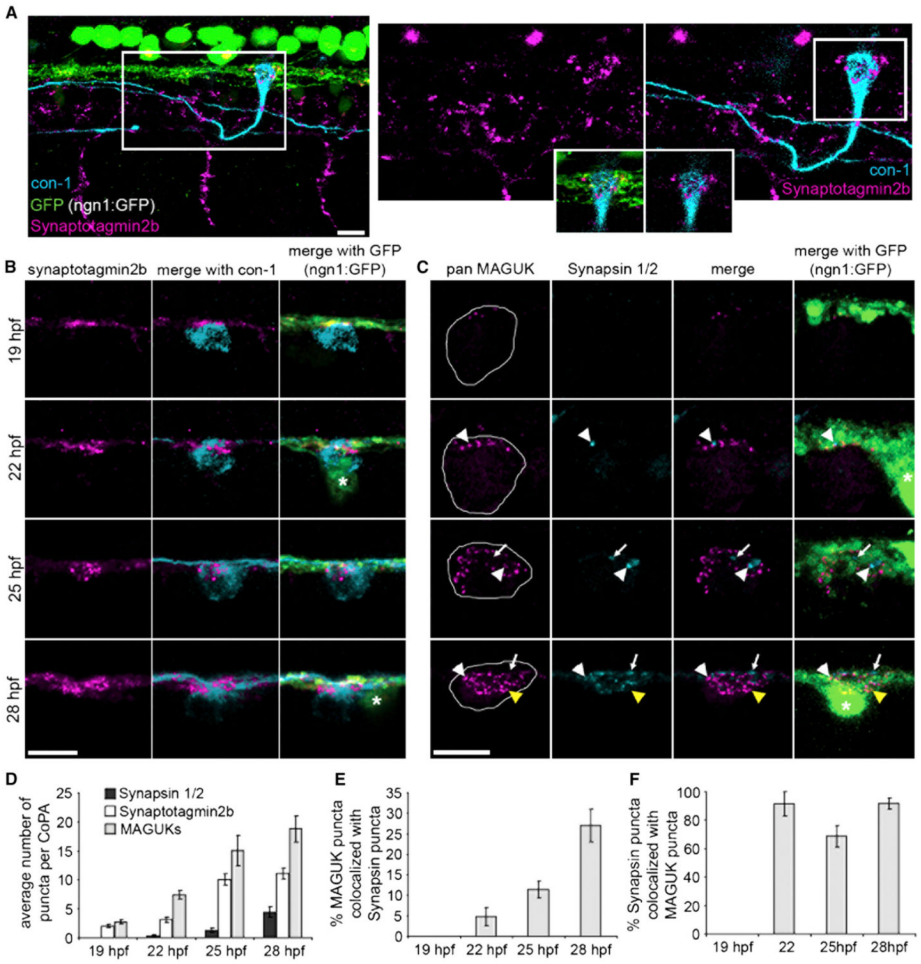

Figure 3. Presynaptic Components Arrive Sequentially during Development

(A) Left panel: lateral view of three segments of a 25 hpf embryo expressing ngn1:GFP (green) labeled with antibodies to synaptotagmin2b (magenta) and CoPA neurons (con-1, cyan). Notice synaptotagmin2b puncta were colocalized with CoPA cell bodies at the dlf. Right panels: zoom of box in left panel. Inset shows single plane of boxed region at the level of the dlf and the contacting region of the CoPA cell. Scale bar represents 10 μm.

(B) Dorsal view of IF labeling for synaptotagmin2b (magenta) colocalized with CoPA cell bodies (cyan) inngn1:GFP embryos from 1–28 hpf. Asterisk labels RB cell bodies. Scale bar represents 10 μm.

(C) Dorsal view of IF labeling for MAGUKs (magenta) and synapsin 1/2 (cyan) from 19–28 hpf. Asterisk labels RB cell bodies. White arrowheads show sites of colocalization of synapsins and MAGUKs, white arrows indicate localization of synapsins only, and yellow arrowheads indicate localization of MAGUKs only. Outlines of CoPA cell bodies were generated by increasing the gain of the MAGUK IF. Scale bar represents 10 μm.

(D) Histogram shows the number of synapsin 1/2, synaptotagmin2b, and MAGUK puncta per CoPA cell from 19–28 hpf.

(E andF) Histograms show the percentage of MAGUK punctacolocalized with synapsin puncta, and the percentage of synapsin puncta colocalized with MAGUK puncta, respectively, from 19–28 hpf. Error bars show SEM. See also Figure S1 and Table S1.

NIH-PA Author Manuscript

NIH-PA Author Manuscript

NIH-PA Author Manuscript

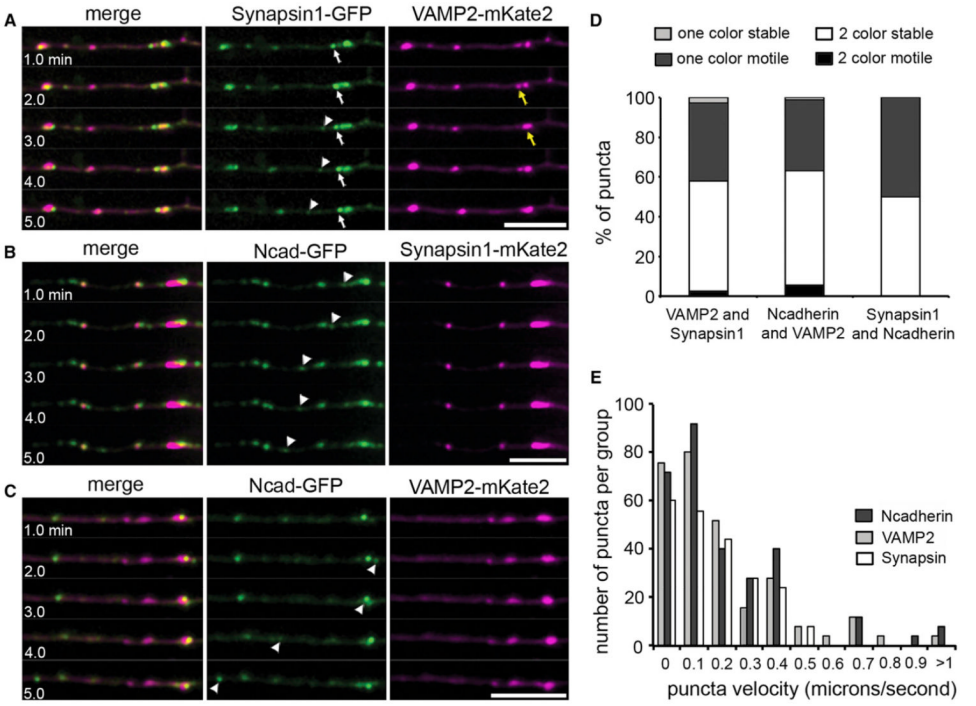

Figure 4. Synapsin1, STVs, and PTVs Are Transported Independently of Each Other

(A–C) Selected sequence of five frames, 1 min apart, from 30 min time-lapse movies showing differential transport of synapsin1-GFP and VAMP2-mKate2 (A), synapsin1-mKate2 and N-cadherin-GFP (B), and N-cadherin-GFP and VAMP2-mKate2 (C) in RB axons. Movies acquired between 24–26 hpf. Arrows and arrowheads highlight motile puncta that were positive for only one of the two fluorescent fusion proteins. A VAMP2-mKate punctum was initially paused (yellow arrow in A) and colocalized with a synapsin1-GFP punctum (white arrow), but then moved away (t = 3.0). Scale bars represent 10 μm.

(D) Histogram showing the number of two color puncta versus single color puncta that are motile over a 30 min imaging period. Two color puncta are those labeled for both transport packet markers imaged in a given pair, single color puncta are those expressing only one of the two markers. Error bars represent SEM. *$p < 0.005$.

(E) Distribution of the number of each type of puncta (N-cadherin, VAMP2, synapsin) at each velocity. The maximum velocity measured for a synapsin1 puncta was 2.49- and 1.98-fold slower than the maximum velocity for an N-cadherin or a VAMP2 puncta, respectively. See also Figure S2 and Movie S2.

NIH-PA Author Manuscript
NIH-PA Author Manuscript
NIH-PA Author Manuscript

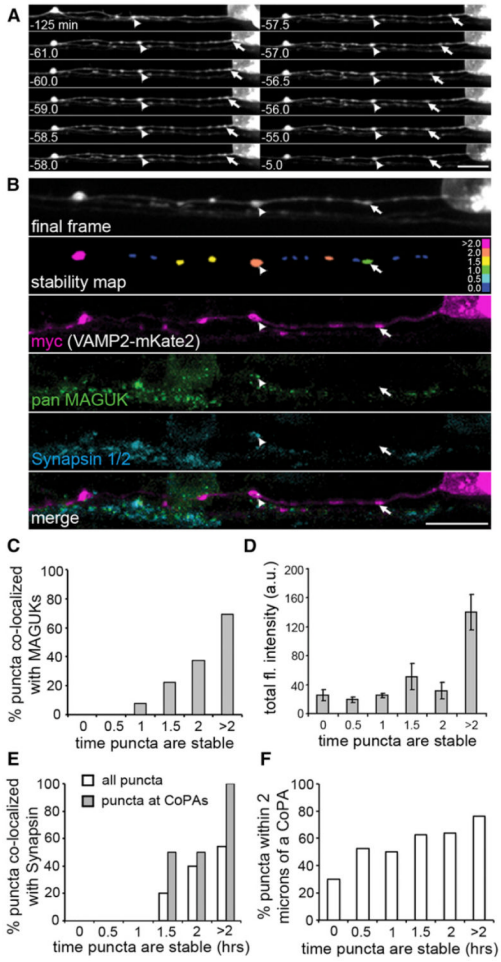

Figure 5. Delayed Synapsin Recruitment to Paused VAMP2-mKate2 Puncta

(A) Selected frames from a 2 hr time-lapse movie (from 24–26 hpf) of VAMP2-mKate2 expressed by a RB cell. Although some puncta remained stable for the entire imaging period (arrowheads) others stabilized during imaging (arrow). Scale bar represents 10 μm.

(B) Postimaging IF labeling demonstrates the presence of MAGUKs (green) at a VAMP2-mKate2 punctum that was paused for at least 2 hr (arrowhead), but not at a punctum paused for 29 min (arrow). The stability map uses a color code to report the time each punctum was paused before the end of imaging. Bins were as follows: nonpaused puncta (0.0, dark blue), paused for 0–0.5 hr (0.5), 0.5–1 hr (1), etc. to puncta paused for the entire imaging period (>2.0, magenta). Scale bar represents 10 μm.

(C) Stability histogram shows quantification of the percentage of VAMP2-mKate2 puncta colocalized with MAGUKs over the total of all axon segments analyzed. Bins are as described for the stability map above. n = 7 RB axon segments analyzed.

(D) Intensity histogram shows the total fluorescence intensity for VAMP2 puncta. A significant increase in total fluorescence intensity was seen at puncta paused for >2 hr. Error bars show SEM.

(E) A stability histogram quantifying the percentage of synapsin 1/2 that colocalized with VAMP2-mKate2 puncta reveals that, on average, recruitment of VAMP2-mKate2 preceded that of synapsin by 83.7 min (±12.5 min). n = 13 RB axon segments analyzed.

(F) A stability histogram quantifying the percentage of VAMP2-mKate2 puncta that are localized within 2 μm of a CoPA cell.

NIH-PA Author Manuscript

NIH-PA Author Manuscript

NIH-PA Author Manuscript

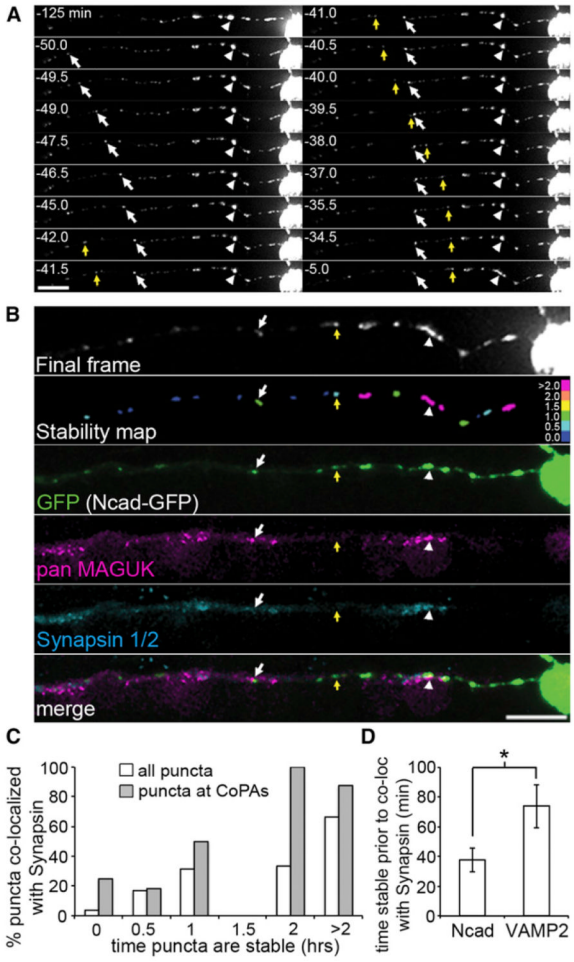

Figure 6. N-Cadherin Recruitment Precedes Synapsin

(A) Selected frames from a 2 hr time-lapse movie (from 24–26 hpf) of Ncad-GFP expression in a RB cell. Some puncta were paused for the entire imaging period (arrowhead), whereas others paused during imaging (arrow). Scale bar represents 10 μm.

(B) Postimaging IF labeling demonstrates the presence of synapsin 1/2 (cyan) and MAGUKs (magenta) at an N-cadherin-GFP (green) punctum that was paused for the entire imaging period (arrowhead) and for 34.5 min preceding the end of imaging (arrow), but not at a punctum that was paused for only 29.5 min preceding the final frame (yellow arrow). A stability map (with bins as described in Figure 5) reports the time each puncta was paused preceding the end of imaging. Scale bar represents 10 μm.

(C) A stability histogram quantifying the percentage of synapsin 1/2 puncta that colocalized with N-cadherin-GFP (white bars) reveals that recruitment of N-cadherin precedes synapsinby 37.6 min (±8.0 min). Gray bars show data for VAMP2-mKate2 from histogram in Figure 5C to emphasize the difference in the time delay with which synapsin colocalization is first seen. Bins were as described for Figure 5.

(D) Histogram quantifying the average amount of time (in min.) NCad and VAMP2 puncta were stable prior to the end of imaging and colocalized with synapsin. n = 13 RB axon segments analyzed. Error bars show SEM. *$p < 0.05$.

NIH-PA Author Manuscript

NIH-PA Author Manuscript

NIH-PA Author Manuscript

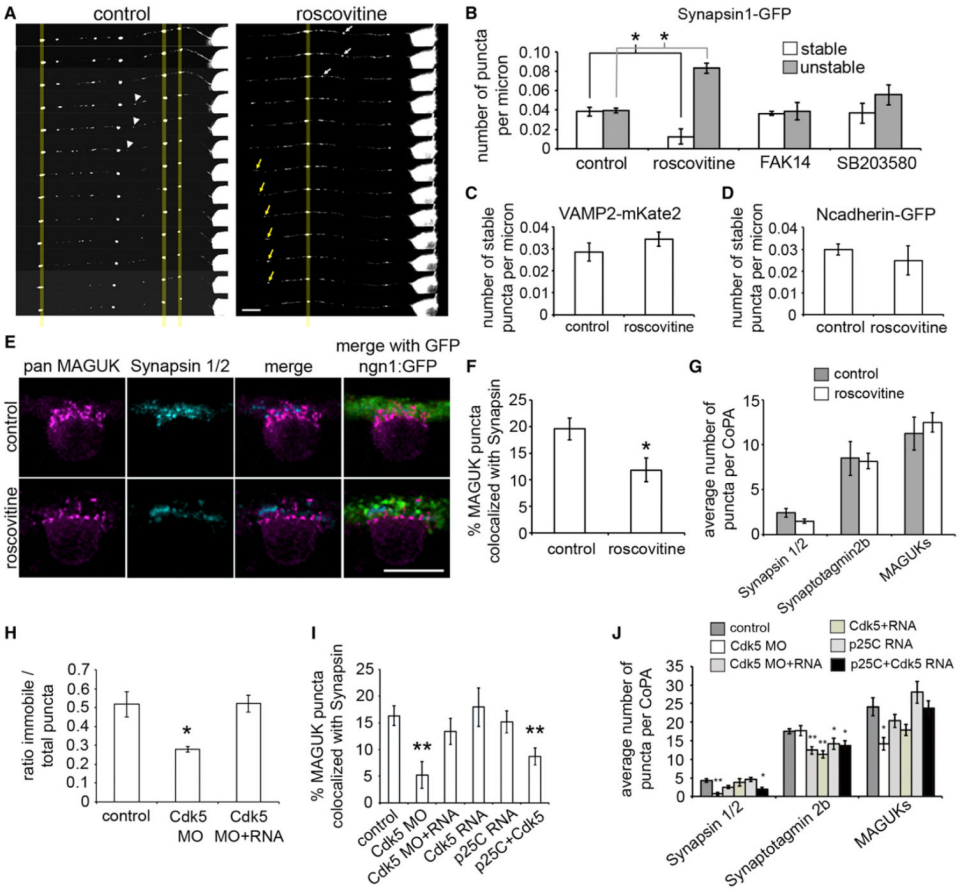

Figure 7. Cdk5 Regulates Synapsin Stabilization at Synapses

(A) Selected frames from 1 hr time lapse movies of synapsin1-GFP expressing RB axons treated with either vehicle (control, left panel) or roscovitine (right panel). Scale bar represents 10 μm.

(B) Histogram quantifying the number of stable and unstable puncta per micron for each treatment condition.

(C and D) Histograms showing the number of stable puncta per micron in control and roscovitine treatment condition sinVAMP2-mKate2 expressing RB axons (C) and in N-cadherin-GFP expressing axons (D).

(E) Dorsal view of IF labeling in 26 hpf ngn1:GFP (green) expressing embryos with antibodies for pan MAGUK (magenta) and synapsin 1/2 (cyan). Scale bar represents 10 μm.

(F) Histogram showing the percentage of MAGUK puncta colocalized with synapsin puncta.

(G) Histogram showing the average number of synapsin 1/2, synaptotagmin2b, and MAGUK puncta per CoPA cell for both control and roscovitine treatment conditions.

(H) Histogram showing the ratio of stable to total synapsin1-GFP puncta in control, Cdk5 MO, and Cdk5 MO and RNA-injected embryos.

(I) Histogram showing the percentage of MAGUK puncta colocalized with synapsin puncta in control, Cdk5 MO, Cdk5 MO and RNA, Cdk5 RNA, p25C RNA, and p25C and Cdk5 RNA-injected embryos.

(J) Histogram showing the average number of synapsin 1/2, synaptotagmin2b, and MAGUK puncta for control, Cdk5 MO, Cdk5 MO and RNA, Cdk5 RNA, p25C RNA, and p25C and Cdk5 RNA-injected embryos. Error bars show SEM. *$p < 0.05$ and **$p < 0.005$ as compared to control condition.